Entanglement in Regge scattering using the AdS/CFT correspondence

Yizhuang Liu[*]
Tsung-Dao Lee Institute, Shanghai Jiao University, Shanghai, 200240, China

Ismail Zahed[†]
Department of Physics and Astronomy, Stony Brook University, Stony Brook, New York 11794-3800, USA

(Received 6 April 2018; revised manuscript received 7 June 2019; published 6 August 2019)

The eikonalized parton-parton scattering amplitude at large $\sqrt{s}$ and large impact parameter, is dominated by the exchange of a hyperbolic surface in walled AdS. Its analytical continuation yields a world sheet instanton that is at the origin of the Reggeization of the amplitude and a thermallike quantum entropy $\mathcal{S}_T$. We explicitly construct the entangled density matrix following from the exchanged surface, and show that its von-Neumann entanglement entropy $\mathcal{S}_E$ coincides with the thermallike entropy, i.e., $\mathcal{S}_T = \mathcal{S}_E$. The ratio of the entanglement entropy to the transverse growth of the exchanged surface is similar to the Bekenstein entropy ratio for a black hole, with a natural definition of saturation and the on-set of chaos in high energy collisions. The largest eigenvalues of the entangled density matrix obey a cascade equation in rapidity, reminiscent of nonlinear QCD evolution of wee-dipoles at low-x and weak coupling. We suggest that the largest eigenvalues describe the probability distributions of wee-quanta at low-x and strong coupling that maybe measurable at present and future pp and ep colliders.

DOI: 10.1103/PhysRevD.100.046005

I. INTRODUCTION

Entanglement in quantum mechanics is still one of the most subtle concept that permeates our description of the quantum world. The canonical example is the entangled Einstein-Podolsky-Rosen pair whereby the measurement of one of the state in the pair forces the state of the partner. This conundrum has recently been revisited in many areas of physics, ranging from low-dimensional quantum critical systems [1,2] to wormholes in gravity [3,4].

Recently the holographic principle was used to derive the entanglement of boundary conformal field theories in terms of pertinent area of finite dimensional surfaces in bulk [5], reviving the idea that the entanglement entropy bears similarities with the Bekenstein entropy for black holes [6]. These relationships are important in our understanding of the concept of information storage or loss whether in quantum mechanics or around a black hole.

Current high multiplicity pp collisions at collider energies display rapid collectivization [7], an indication of early entropy deposition and thermalization. This leads us to ask about the origin of this fast scrambling of information in the prompt phase of the process. One of the purpose of this paper is to show that parton-parton scattering at large $\sqrt{s}$ is highly entangled, with an entanglement entropy matching the thermodynamical entropy initially discussed in [8]. Entanglement entropies in the context of perturbative QCD evolution were recently discussed in [9,10].

Below we briefly review the Reggeization of the parton-parton scattering at large $\sqrt{s}$, through the exchange of a minimal surface using the AdS/CFT correspondence. The transverse fluctuations on the surface are shown to be entangled with an entropy that equals that of critical conformal field theories in lower dimension. The largest eigenvalues of the entangled density matrix describe the probability distributions of wee-quanta at low-x and strong coupling.

II. REGGEIZED SCATTERING FROM AdS/CFT

Elastic hadron-hadron and lepton-hadron collisions at large $\sqrt{s}$ are dominated by Pomeron and Reggeon exchanges [11,12]. Perturbative QCD evolution describes these exchanges through ordered gluon ladders [13,14], while nonperturbative holographic descriptions suggest string exchanges [15–18] or Reggeized bulk gravitons [19]. Throughout, we will present the holographic string version. A brief review of this approach will be given in this section.

[*]yizhuang.liu@sju.edu.cn
[†]ismail.zahed@stonybrook.edu

A. Motivation

At large N_c, QCD processes are dominated by planar graphs. In the Pomeron limit with $s \gg -t$, the scattering between a pair dipoles DD or quarks $Q\bar{Q}$ is characterized by the exchange of planar graphs which can be regarded as the exchange of a closed string (Pomeron) or an open string (Reggeon). In the holographic limit of a large number of colors and strong coupling $N_c \gg \lambda \gg 1$, the exchanged gluons are qualitatively ordered as suggested in [20].

For an intuitive understanding of this ordering, it is best to consider the original Maldacena's modified Coulomb law [21]. For that, consider the ordered gluon contribution for the potential between two heavy quarks as illustrated in Fig. 2. In Feynman gauge where the retardation is manifest, the ordered gluons contribute to the potential as

$$V(b) = -\frac{\lambda}{4\pi^2}\int \frac{dt_{12}}{t_{12}^2 + b^2} \tag{1}$$

In the Abelian case, the interaction takes place at all virtualities with typically the dominant and large times $\Delta t_{12} \sim b$, leading to the standard Coulomb potential $V(b) \sim -\lambda/b$. At strong coupling, the non-Abelian modified Coulomb law is seen to be dominated by short time exchanges $\Delta t_{12} \sim b/\sqrt{\lambda} \ll b$, with (1) giving

$$V(b) \sim -\frac{\lambda \Delta t_{12}}{b^2} \sim -\frac{\sqrt{\lambda}}{b} \tag{2}$$

At strong coupling, the coherence captured by the potential can only build if the exchanged non-Abelian gluons travel superluminally, for otherwise they will undergo multiple splitting and lose coherence because of the large gauge coupling λ. These rapid exchanges are suggestive of the ordering in Figs. 1,2. We emphasize the qualitative and intuitive character of this argument, which does not allow for fixing the overall coefficient in (2) for instance.

B. Eikonal amplitude

In the eikonal limit, the probe and target partons support Wilson lines running along the light cone and sourcing

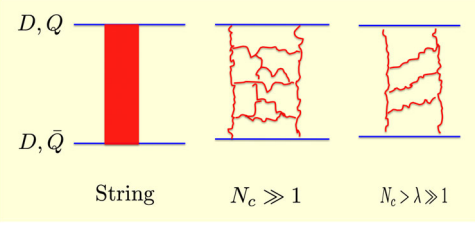

FIG. 1. Schematic description of the string exchange in large N_c (planar graphs) and holographic limit (ordered ladders) between a pair of dipoles (DD) or partons ($Q\bar{Q}$). See text.

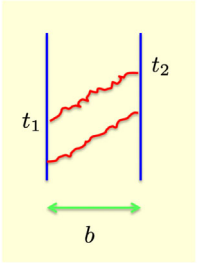

FIG. 2. Ordered exchange at strong coupling.

gluon fields [22]. Specifically, the parton-parton scattering amplitude at large N_c, is given by ($t = -\mathbf{q}^2$)

$$\mathcal{T}_{ij,kl}(s,t) = -2is\int d\mathbf{b}\, e^{i\mathbf{q}\cdot\mathbf{b}}\mathbf{WW}_{ij,kl}, \tag{3}$$

with the connected Wilson loop correlator

$$\mathbf{WW}_{ij,kl} \equiv \langle \mathbf{W}_{ij}(C_1)\mathbf{W}_{kl}(C_2)\rangle_{\rm con} \tag{4}$$

traced over colors, and subject to the normalization $\langle \mathbf{W}_{ii}\rangle = N_c$. The Wilson lines $\mathbf{W}_{ij}$ are evaluated along $C_{1,2}$ on the light cone at fixed separation $b = |\mathbf{b}|$

$$\mathbf{W}_{ij}(C_{1,2}) = (\mathbf{P}e^{ig\int_{C_{1,2}} A})_{ij} \tag{5}$$

as illustrated in Fig. 3 following [15,16,22]. The averaging in (4) is over the Yang-Mills gauge fields. The integrand in (3) is the impact parameter representation of the scattering amplitude in the s-channel.

Vacuum gauge invariance allows the decomposition of (3) into a singlet and octet contribution

$$\mathcal{T}_{ij,kl} = \mathcal{T}_0\delta_{ij}\delta_{kl} + \mathcal{T}_{N_c^2-1}T^a_{ij}T^a_{kl} \tag{6}$$

where T^a are the generators of SU(N_c) in the fundamental representation. Each of the amplitudes in (6) can be obtained by a pertinent closing of the $C_{1,2}$ contours at infinity, leading to

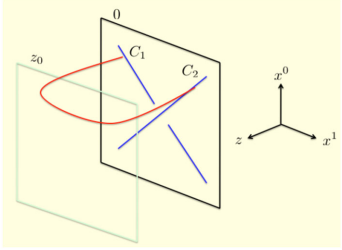

FIG. 3. Wilson lines with the attached string $0 \le z \le z_0$.

$$\mathcal{T}_0 = \frac{1}{N_c^2}\langle \mathbf{W}\mathbf{W}_{ii,jj}\rangle - 1$$
$$\mathcal{T}_0 + \frac{N_c^2-1}{2N_c}\mathcal{T}_{N_c^2-1} = \frac{1}{N_c}\langle \mathbf{W}\mathbf{W}_{ij,ji}\rangle - 1. \quad (7)$$

Both the singlet and octet amplitudes are gauge invariant and can be assessed using perturbative or nonperturbative arguments. We choose to evaluate them using nonperturbative arguments in the context of holography which we now present.

C. Holography

In the holographic limit, these gauge invariant amplitudes are dominated by string exchanges. In leading order, the correlator of Wilson lines involve surface exchange in a slice of AdS with a metric

$$ds^2 = \frac{R^2}{z^2}(-dt^2 + dz^2 + dx^i dx^i) \quad (8)$$

for $0 \le z \le z_0$ with $D_\perp = 3$. The invariant correlators in (7) are dominated by the minimal surface attached to $C_{1,2}$ [21]

$$\mathbf{W}\mathbf{W} \sim e^{-\sigma_T \mathcal{A}_{\min}} \equiv e^{-S_{\min}} \quad (9)$$

The singlet amplitude involves the exchange of a closed surface with the topology of a cylinder, while the octet amplitude involves the exchange of an open surface with the topology of a disc, as discussed in [15–18]. Here, we present a simplified analysis where the inelasticity carried by the exchanged surfaces is encoded in a generic world sheet instanton irrespective of the topology of the surface.

Consider the open string exchange. For large impact parameter b, the extremal surface is composed of two straight strips joined by a surface at $z = z_0$ as shown in Fig. 3. The two straight strips contribute about 1 in (7) with the normalization $\langle \mathbf{W}_{ii}\rangle = N_c$. To assess the joining surface at $z = z_0$ where the metric is nearly flat, we use the Polyakov action in the *conformal* gauge with mostly positive Minkowski signature ($a = \tau, \sigma$)

$$S = \frac{\sigma_T}{2}\int_0^T d\tau \int_0^1 d\sigma \partial_a x \cdot \partial_a x + \text{b.c.} \quad (10)$$

with the string tension

$$\sigma_T = \frac{R^2}{(2\pi\alpha'_{\mathbb{X}} z_0^2)} \sim \frac{\sqrt{\lambda}}{(2\pi z_0^2)} \quad (11)$$

Our treatment of the closed ($\mathbb{X} = \mathbb{P}$) and open ($\mathbb{X} = \mathbb{R}$) topologies will be similar except for: 1/ an adjustment of the string tension by choosing

$$\alpha'_{\mathbb{P}} = \frac{1}{2}\alpha'_{\mathbb{R}} \equiv \alpha', \quad (12)$$

and 2/ an additional $\frac{1}{s}$ suppression of the scattering amplitude (3) for he open surface exchange due to the running quark lines on the open boundary [23]. Throughout we will set $R = z_0$.

For large b, the boundary conditions at $z = 0$ transfer almost unchanged to $z = z_0$. These boundaries are straight lines with rapidity angles $\chi/2$ and $-\chi/2$ for $\sigma = 0$, 1 respectively, with $\chi = \ln s \gg 1$. At $\sigma = 0$ we have [17]

$$\cosh(\chi/2)\partial_\sigma x^0 + \sinh(\chi/2)\partial_\sigma x^1 = 0,$$
$$\sinh(\chi/2)\partial_\tau x^0 + \cosh(\chi/2)\partial_\tau x^1 = 0, \quad (13)$$

and similarly at $\sigma = 1$. The extremal solution to (10) with $\partial_a^2 x = 0$ and subject to (13) at $z = z_0$, is the hyperbolic surface ($\bar\sigma = \sigma - \frac{1}{2}$)

$$(x^0, x^1, x^\perp, z) = \left(\frac{b}{\chi}\cosh(\chi\bar\sigma)\sinh(\chi\tau), \frac{b}{\chi}\sinh(\chi\bar\sigma)\sinh(\chi\tau), b\sigma, z_0\right). \quad (14)$$

The induced world-sheet metric associated to (14) is conformal,

$$ds_W^2 = b^2\cosh^2(\chi\tau)(-d\tau^2 + d\sigma^2) \quad (15)$$

which is consistent (*a posteriori*) with the gauge choice in (10). It is free of the wormhole discussed in [4]. Using the analytical continuation $\tau \to i\tau$, we have

$$ds_W^2 \to b^2\cos^2(\chi\tau)(d\tau^2 + d\sigma^2) \quad (16)$$

which describes the conformal world sheet of an "*instanton*" with period $T_P = 2\pi/\chi \ll 1$ and finite action

$$S_{\min} = \sigma_T \int_0^{T_P} b^2\cos^2(\chi\tau)d\tau \int_0^1 d\sigma = \frac{1}{2}\sigma_T(bT_P)b. \quad (17)$$

From (12), it follows that the world sheet instanton contribution for the Pomeron is twice that of the Reggeon with $\sigma_{\mathbb{P}} = 2\sigma_{\mathbb{R}}$ and $S_{\mathbb{P}} = 2S_{\mathbb{R}}$. The closed surface exchange can be thought as two glued open surface exchanges. In Fig. 4 we give an illustration of the geometrical relationship between the worldsheet instanton and the hyperbolic surface sustained by the nearly eikonal trajectories. A more thorough characterization of this instanton and its relation to the Schwinger mechanism on the world sheet can be found in [17] (see Sec. III D).

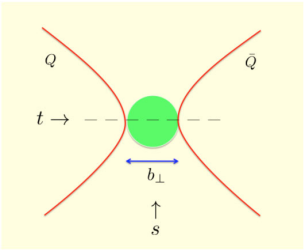

FIG. 4. Eikonal scattering with the instanton exchange.

D. Reggeized amplitude

Following the AdS/CFT correspondence, we insert (17) into (10) and define $\beta = bT_P$, to obtain (9) as

$$\mathbf{WW} \sim e^{-S_{\min}-S_{1\text{loop}}} = e^{-\frac{1}{2}\sigma_T\beta b+\frac{D_\perp}{12}\chi} = e^{-\frac{b^2}{2\alpha'_{\mathbb{X}}\chi}+\frac{D_\perp}{12}\chi}. \tag{18}$$

We have included the 1-loop quantum correction restricted to the world sheet instanton strip $b \times \beta$. For $\chi \gg 1$, the strip is highly elongated $b \gg \beta$ and *periodic* in β. The 1-loop contribution is dominated by the Casimir energy or Luscher term [24]

$$S_{1\text{loop}} = \frac{D_\perp}{2}\ln\det(-\partial_\perp^2) = -\frac{\pi D_\perp}{6}\frac{b}{\beta} = -\frac{D_\perp}{12}\chi. \tag{19}$$

Inserting (18) in (3) and carrying the transverse Fourier transform yields the Reggeized scattering amplitude $\mathcal{T}_{\mathbb{X}} \sim is^{\alpha_{\mathbb{X}}(t)}$ $(R = z_0)$

$$\alpha_{\mathbb{P}}(t) = 1 + \frac{D_\perp}{12} + \frac{\alpha'}{2}t$$
$$\alpha_{\mathbb{R}}(t) = 1 - 1 + \frac{D_\perp}{12} + \alpha' t \tag{20}$$

in agreement with [17] (see Sec. IV) for the Pomeron, and with [23] for the Reggeon. Note the -1 from the additional $\frac{1}{s}$ suppression in this channel as stated earlier.

E. Warped Gribov diffusion

To exponential accuracy, (18) happens to be exactly the tachyon-mode contribution to the closed string propagator subject to the twisted boundary conditions (13). Specifically, in the Pomeron channel the exact tachyon contribution is [18,25]

$$\mathbb{K}_0(t_\chi, b) = \left(\frac{1}{4\pi t_\chi}\right)^{\frac{D_\perp}{2}} e^{-\frac{b^2}{4t_\chi}+\frac{D_\perp t_\chi}{6\alpha'}} \sim \mathbf{WW} \tag{21}$$

with the rapidity playing the role of time

$$t_\chi = \frac{\alpha'}{2}\chi \equiv D_{\mathbb{P}}\chi \tag{22}$$

and $D_{\mathbb{P}}$ playing the role of a diffusion constant. For large rapidity $\chi \gg 1$, all other string excitations are suppressed. The world sheet instanton in (18) captures semiclassically the tachyon contribution in (21).

(21) embodies the famed Gribov diffusion,

$$\partial_{t_\chi}\mathbb{K}_0 + (M_0^2 - \nabla_\perp^2)\mathbb{K}_0 = 0 \tag{23}$$

with the tachyon mass $M_0^2 = -D_\perp/6\alpha'$. It acts as a *source* term in the diffusion process. The Pomeron intercept, the Luscher term and the tachyon mass are intimatly related in our analysis. It is now clear, that the effects of warping amount to a warped Gribov diffusion

$$\partial_{t_\chi}\mathbb{K}_0 + \left(M_0^2 - \frac{1}{\sqrt{g_\perp}}\partial_\mu g_\perp^{\mu\nu}\sqrt{g_\perp}\partial_\nu\right)\mathbb{K}_0 = 0 \tag{24}$$

with $g_\perp$ the transverse AdS-metric. The transverse directions include the holographic z-direction, so that $\mathbb{K}_0(t,b) \to \mathbb{K}_0(t,b,z)$ as $z = z_0$ is now relaxed. For AdS the solution to (24) can be obtained in closed form. Specifically, for $z \ll b$ and $\mathbf{D}_\perp = \mathbf{3}$ we have [18] [see Eq. (38)]

$$\frac{1}{zz_0}\mathbb{K}_0(t_\chi, b, z) \approx \frac{e^{(\alpha_{\mathbb{P}}(0)-1))}}{(4\pi t_\chi)^{\frac{3}{2}}}\frac{2z}{z_0 b^2}\ln\left(\frac{b^2}{zz_0}\right)e^{-\frac{1}{4t_\chi}\ln^2(\frac{b^2}{zz_0})}. \tag{25}$$

Modulo the string parameters $\alpha_{\mathbb{P}}$ and $D_{\mathbb{P}}$, (25) is identical to Mueller's Balitsky-Fadin-Kuraev-Lipatov density of wee-dipoles of size z in onium-onium scattering in the 1-Pomeron approximation at weak coupling [26] [see Eq. (8) in Sec. II].

Remarkably, (24) interpolates between the scattering amplitude of the soft Pomeron (21) and the hard Pomeron (25) in impact parameter space for exactly $\mathbf{D}_\perp = \mathbf{3}$. Therefore, it is natural to interpret the string zero point fluctuations in the exchanged instanton world sheet as wee-dipoles at strong coupling, much like Mueller's wee-dipoles at weak coupling. We will return to this point below.

III. THERMALLIKE ENTROPY

The exchanged instanton period or tunneling time, plays the role of an inverse temperature for the zero point fluctuations on the induced world sheet

$$\beta = bT_P = \frac{2\pi b}{\chi}. \tag{26}$$

This temperature is kinematical in origin, as it arises from the rapidity χ of the colliding pairs for fixed impact parameter b. The larger the rapidity and/or smaller the

impact paramer, the shorter the tunneling time or higher the temperature.

This physical observation is important. It shows that the Casimir energy or Luscher term in (19) is the *free energy* $\mathcal{F}_T$ of $D_\perp$ massless bosons confined to a 1-dimensional box of length b at temperature $1/\beta$,

$$\begin{aligned}\beta\mathcal{F}_T &= D_\perp \int \frac{bdp}{2\pi} \ln(1-e^{-\beta|p|}) \\ &= -\frac{\pi D_\perp}{6}\frac{b}{\beta} \\ &= S_{1\text{loop}}. \end{aligned} \tag{27}$$

The zero point fluctuations on the instanton world sheet are *thermallike* Hence, the exchanged instanton plus zero-point motion carry a thermal entropy $\mathcal{S}_T$ that follows from standard thermodynamics

$$\begin{aligned}\mathcal{S}_T &= \frac{\beta\partial\mathcal{F}_T}{\partial\ln\beta} \\ &= D_\perp \int \frac{bdp}{2\pi}\frac{2\beta|p|}{e^{\beta|p|}-1} \\ &= \frac{D_\perp}{6}\chi = 2(\alpha_{\mathbb{P}}(0)-1)\chi \end{aligned} \tag{28}$$

in agreement with the initial observation in [8,25]. The thermallike entropy (28) per unit rapidity χ is fixed by the Pomeron intercept $\alpha_{\mathbb{P}}(0)$. It is at the origin of the rise of the scattering cross section and ultimately the multiplicities in high energy scattering as discussed in [8,25].

IV. ENTANGLEMENT ENTROPY

In this section we show that the string thermallike entropy $\mathcal{S}_T$ in (28) is *identical* to the entanglement von Neumann entropy $\mathcal{S}_E$ following from the blocked density matrix of the transverse part of the exchanged string. The longitudinal part of the string freezes out due to Lorentz contraction at large rapidity. Throughout this section we will set $\alpha' = \frac{1}{4}$, and reinstate it when needed by inspection.

A. Transverse Hamiltonian

The transverse fluctuations at the origin of (19)–(28) are associated to the Polyakov action (10) with $x \to x_\perp$ and fixed endpoints around the hyperbolic configuration (14),

$$S_\perp = \frac{\sigma_T}{2}\int_0^T d\tau \int_0^1 d\sigma(\dot{x}_\perp{}^2 - x'_\perp{}^2) + \text{b.c.} \tag{29}$$

The action density can be thought as that of a collection of N strings connected by identical springs for $z = z_0$, and discretized as follows [27–29]

$$\frac{1}{N}\sum_{k=0}^{N}(\dot{x}^i_\perp(k))^2 - \frac{1}{N}\sum_{k=1}^{N}\left(\frac{x^i_\perp(k)-x^i_\perp(k-1)}{\frac{\pi}{N}}\right)^2 \tag{30}$$

where the summation over $i = 1,\ldots,D_\perp$ is subsumed. Note that (30) reduces to (29) as $N \to \infty$. (30) describes N coupled harmonic oscillators in $D_\perp$ dimensions, with a transverse Hamiltonian

$$\frac{2}{N}\mathbb{H}_\perp = \frac{1}{2}\sum_{k=0}^{N}(p^i_k)^2 + \frac{1}{2}\sum_{k,l=1}^{N} x^i_k \mathbb{K}_{kl} x^i_l \tag{31}$$

where $\mathbb{K}$ is a banded matrix

$$\mathbb{K}_{kl} = \frac{4}{\pi^2}(2\delta_{kl} - \delta_{k,l+1} - \delta_{k,l-1}) \tag{32}$$

with positive eigenvalues. Ignoring warping at large b, the ground state wave function of (31) is

$$\Psi[x] = \left(\frac{|\Omega|}{\pi^N}\right)^{\frac{D_\perp}{4}} e^{-\frac{1}{2}\sum_{k,l=1}^{N} x^i_k \Omega_{kl} x^i_l} \tag{33}$$

where Ω is the square root of $\mathbb{K}$.

Since $\mathbb{K}$ is real symmetric, it diagonalizes by orthogonal rotation with $\mathbb{K} = U^\dagger K_D U$ and $\Omega = U^\dagger\sqrt{K_D}U$. The eigenvalues and eigenvectors of $\mathbb{K}$ are respectively

$$\begin{aligned}\lambda_k &= \frac{8}{\pi^2}\left(1-\cos\frac{\pi k}{2p+1}\right) \\ \alpha^n_k &= \sqrt{\frac{2}{2p+1}}\sin\frac{\pi k n}{2p+1} \end{aligned} \tag{34}$$

with k labeling the eigenvalues and n labeling the entries, $k, n = 1, 2, \ldots 2p$. The matrices U, Ω can be found in explicit form, with $U_{kn} = \alpha^n_k$ and

$$\Omega_{mn} = \sum_{s=\pm}\frac{sC}{\cos\frac{\pi(m-sn)}{2p+1} - \cos\frac{\pi}{4p+2}} \tag{35}$$

with C an overall unimportant constant. Given Ω_{mn}, the derivation of the entanglement entropy is essentially an exercise in the diagonalization of nested Gaussians as in [6].

B. Density matrix

The transverse string density matrix is $\Psi[x]\Psi^*[x']$. To quantify the entanglement of the string bits in transverse space, we follow Srednicki [6] and define the entanglement density

$$\rho_E[\bar{x},\bar{x}'] = \int d[\underline{x}]\Psi[\underline{x},\bar{x}]\Psi^*[\underline{x};\bar{x}'] \tag{36}$$

where we used the notation $[x] \to [\underline{x}; \bar{x}]$ with $\dim \underline{x} = n$ and $\dim \bar{x} = N - n$. The positive eigenvalues of (36) follow by diagonalization

$$\int d[\bar{x}'] \rho_E[\bar{x}, \bar{x}'] \varphi_l[\bar{x}'] = p_l \varphi_l[\bar{x}]. \tag{37}$$

The entanglement entropy is the Von-Neumann entropy for the transverse string

$$\mathcal{S}_E(n, N) = -\sum_{l=0}^{\infty} p_l \ln(p_l). \tag{38}$$

C. Von-Neumann entropy

For the 2 limiting cases $n = 1$ and $n = N/2$ (38) can be obtained in closed form. For general n the eigenvalues p_l can only be obtained numerically. For that, we fix the endpoints through the boundary condition $x_{N+1} = x_1 = 0$. Without loss of generality, we set $N = 2p$ and subdivide N into

$$[N] = [n] \cup [N - n]. \tag{39}$$

The entanglement entropy between the subsystem with size $[n]$ and the one with size $[N - n]$ can be calculated by splitting the matrix Ω in (35) as

$$B_{N,n} = \Omega_{m\bar{m}}, \qquad m \in (1, \ldots n), \qquad \bar{m} \in (n + 1, \ldots N) \tag{40}$$

and defining the squared matrix $\tilde{\beta}$ through

$$\beta_{N,n} = \Omega_{N,n}^{-\frac{1}{2}} B_{N,n} \Omega_{N,N-n}^{-1} B_{N,n}^T \Omega_{N,n}^{-\frac{1}{2}} \equiv \Omega_{N,n}^{-\frac{1}{2}} \tilde{\beta}_{N,n} \Omega_{N,n}^{\frac{1}{2}}. \tag{41}$$

The corresponding eigenvalue spectrum follows from

$$\tilde{\beta}_{N,n} v_{N,n,i} = \chi_{N,n,i} v_{N,n,i} \tag{42}$$

with $0 \le i \le n$. For each transverse dimension $1, \ldots, D_\perp$, the eigenvalues of the entangled density matrix (37) are [6]

$$p_l[N, n, i] = (1 - \xi_{N,n,i}) \xi_{N,n,i}^l \tag{43}$$

with

$$\xi_{N,n,i} = \frac{\chi_{N,n,i}}{\chi_{N,n,i} + \sqrt{1 - \chi_{N,n,i}^2}}. \tag{44}$$

The entanglement entropy (38) is then

$$\begin{aligned} \mathcal{S}_E(n, N) &= -D_\perp \sum_{i=1}^{n} \sum_{l=0}^{\infty} p_l[N, n, i] \ln p_l[N, n, i] \\ &= -D_\perp \sum_{i=1}^{n} \left(\ln(1 - \xi_{N,n,i}) + \frac{\xi_{N,n,i}}{1 - \xi_{N,n,i}} \ln \xi_{N,n,i} \right). \end{aligned} \tag{45}$$

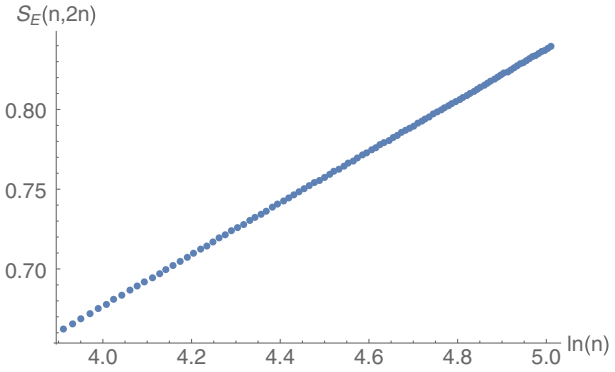

FIG. 5. The entanglement entropy $\mathcal{S}_E(n, 2n)$ per $D_\perp$ versus $\ln(n)$ in the range $50 \le n \le 150$ for a transverse string with fixed ends.

In Fig. 5 we show our results for $\mathcal{S}_E(n, N = 2n)$ versus $\ln(n)$ per $D_\perp$, in the range $50 \le n \le 250$,

$$\mathcal{S}_E(n, N) = \frac{D_\perp}{6} \ln(n) \to \frac{D_\perp}{6} \ln\left(\frac{N}{\pi} \sin\left(\frac{n\pi}{N} \right) \right). \tag{46}$$

Because of the midpoint symmetry of the chain, the last equation follows. We have checked that for the string with periodic boundary conditions, i.e., $x_{N+1} = x_1$, (46) is also recovered with $1/6 \to 1/3$ (2 boundary points). (46) is identical to the thermodynamical entropy (28) for $1 \ll n \ll N$ with the identification of the rapidity $\chi = \ln(n)$ (see below). It is consistent with results from conformal field theories and spin chains with central charge $D_\perp$ [1] (1 boundary point).

D. Black-hole and chaos

With increasing rapidity χ, the exchanged string is longitudinally Lorentz contracted and transversely more elongated and excited causing it to spread. The string transverse squared size is given by the averaging

$$R_\perp^2(N) = \frac{1}{N} \sum_{i=1}^{D_\perp} \sum_{k=1}^{N-1} \langle (x_k^i)^2 \rangle \tag{47}$$

with the probability distribution fixed by (33)

$$|\Psi[x]|^2 = \left| \prod_{i=1}^{D_\perp} \prod_{k=1}^{N} \left(\frac{\sqrt{\lambda_k}}{\pi} \right)^{\frac{1}{4}} e^{-\frac{\sqrt{\lambda_k}}{2} x_k^{i2}} \right|^2. \tag{48}$$

Each of the discretized string bit coordinates x_k^i is normally distributed with probability $|\Psi[x]|^2$. This gives rise to a random walk of the string bits along the chain in the transverse direction with fixed endpoints. The transverse squared size (47) is

$$R_\perp^2(N) = \frac{D_\perp}{2N}\sum_{k=1}^{N-1}\frac{1}{\sqrt{\lambda_k}} \approx \frac{D_\perp}{4}\ln N \to D_\perp \alpha' \ln N \tag{49}$$

after reinstating the units $\frac{1}{4} \to \alpha'$.

This result is consistent with the unwarped Gribov diffusion for the Pomeron, since (21) implies a transverse normal diffusive spread

$$\langle b^2 \rangle = 2D_\perp t_\chi = D_\perp \alpha' \chi \tag{50}$$

with the averaging carried using (21). A comparison of (49) with (50) shows that the number of string bits N and the rapidity of the colliding pair χ, are tied

$$N = e^\chi \tag{51}$$

Recall that the rapidity χ and the Lorentz factor $\gamma = 1/\sqrt{1-\beta^2}$ in the relativistic limit are tied by $\chi = \ln s = 2\ln\gamma$. The more we boost the string, the larger the rapidity χ, the more string bits N in the transverse plane, the longer the intrinsic length $L = N\sqrt{\alpha'}$ of the string.

From (46) it follows that the entanglement entropy growth is proportional to the squared transverse size of the string at the same resolution n

$$\mathcal{S}_E(n) = \frac{\pi R_\perp^2(n)}{6\pi\alpha'}. \tag{52}$$

This is reminiscent of the Bekenstein entropy $S_{\rm BH}$ for a *black hole* in relation to its area $A_{\rm BH}$ [30]

$$S_{\rm BH} = \frac{A_{\rm BH}}{4l_P^2} = \frac{\pi R_{\rm BH}^2}{l_P^2}. \tag{53}$$

In (52) the string length plays the role of an effective Planck length l_P.

Black holes are maximal scramblers. The correspondence between (52) and (53) implies that the entanglement entropy *density* saturates at very large rapidities, with a saturation momentum

$$Q_S^2 = \frac{S_E(n)}{\pi R_\perp^2(n)} = \frac{1}{6\pi\alpha'} \equiv \frac{1}{l_P^2}. \tag{54}$$

This corresponds to 1 unit of entanglement entropy per effective Planck area. For a string length $\sqrt{\alpha'} = 0.1$ fm, the saturation momentum is $Q_S \approx 0.5$ GeV.

We note that in terms of the Gribov diffusionlike time t_χ in (22), the entanglement entropy (28) grows linearly with t_χ. This translates to a constant growth rate

$$\frac{d\mathcal{S}_E}{dt_\chi} = \frac{D_\perp}{3\alpha'} \equiv \kappa_L. \tag{55}$$

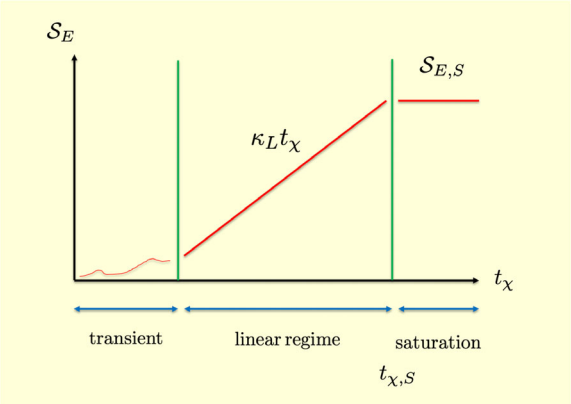

FIG. 6. Typical production of entanglement entropy by evolution in rapidity χ [also $\ln\frac{1}{x}$)] or Gribov time t_χ. See text.

In Fig. 6 we show the typical evolution of the entanglement entropy with rapidity χ, or low-x (see below) or Gribov time. After an initial transient, a linear regime takes place with a characteristic rate κ_L ending in the saturation regime. The typical Gribov time for saturation $t_{\chi,S} \sim \mathcal{S}_{E,S}/\kappa_L$ is reached for a rapidity

$$\chi_S = \left(\frac{6}{D_\perp}\right)\mathcal{S}_{E,S} \to \frac{1}{2(\alpha_{\mathbb{P}}(0)-1)}\mathcal{S}_{E,S}. \tag{56}$$

For pp scattering, $\mathcal{S}_{E,S}$ can be estimated from (53)–(54) in the black disc limit with $\pi R_\perp^2 = 1$ fm^2 and a string length $\sqrt{\alpha'} = 0.1$ fm, i.e., $\mathcal{S}_{E,S} = 100/(6\pi) \approx 5$. For $D_\perp = 3$ the Pomeron intercept is $\alpha_{\mathbb{P}}(0) = 1.25$, this translates to $\chi_S = 10.6$, hence a collision energy $\sqrt{s}/m_N \approx 200$. We note that our estimates are sensitive to the numerical value of the intercept $\alpha_{\mathbb{P}}(0)$.

In general chaotic systems, the growth rate of the entropy in physical time is usually bounded by the Kolmogorov-Sinai entropy rate λ_L, i.e., $|d\mathcal{S}/dt| \le \lambda_L$, with λ_L the sum of all positive Lyapunov exponents [31]. It is a key measure of chaoticity. The above analogy with the black hole suggests that the entanglement production rate (55) is at the *chaos bound*.

By contrast, the classical entropy of the string $\mathcal{S}_S$ grows faster. Specifically, for a string with N-string bits in $D_\perp$ dimensions, the total number of string states are $N_S = D_\perp^N$, and its entropy is then

$$\mathcal{S}_S = \ln N_S = N\ln D_\perp = e^\chi \ln D_\perp. \tag{57}$$

It is proportional to the total mass or length of the string, and grows faster than the quantum entanglement entropy S_E. In terms of the Gribov diffusion time, the corresponding rate is

$$\frac{d\ln\mathcal{S}_S}{dt_\chi} = \frac{1}{D_{\mathbb{P}}} \tag{58}$$

with $D_{\mathbb{P}}$ the Pomeron diffusion constant. The scrambling in Gribov time is now seen to scale logarithmically with $\mathcal{S}_S$. A similar scaling of the scrambling in real time was noted for black holes [32]. The rate (58) violates the Kolmogorov-Sinai bound [31]. Such violations usually occur in a transient regime, as also noted for chaotic maps [31] (second reference). This rapid growth in the classical entropy of the string S_S is expected to stop when string self-interactions are included at saturation [29].

V. WEE-QUANTA

We now show that the largest eigenvalue of the entangled density matrix of the string carries most of the quantum collectivity, and allows for a global characterization of the wee-dipoles or wee-quanta at strong coupling. This discussion offers a complementary view of the Gribov diffusion discussed earlier, where the warped amplitude for the world sheet instanton plus zero point motion was shown to carry identical information to the distribution of Balitsky-Fadin-Kuraev-Lipatov-like wee-dipoles, albeit at strong coupling.

A. Largest eigenvalues

The entanglement entropy is dominated by the largest two eigenvalues $\xi_{N,n,i=1,2}$ with $\xi_{N,n,1} = 0.155\ln(n)$ as shown in Fig. 7, which reproduces the entropy (46) for small $\ln(n)$. The eigenvalue distribution decreases exponentially (Poisson), i.e., $\xi_{2n,n,i>2} \approx e^{-a|i|}$, as shown in Fig. 8 for $2n = 300$ and $a = 3.65$. The dependence of $\xi_{300,n,1}$ on n is shown by the dots on the semicircle like in Fig. 7, with the best fit

$$\xi_{N,n,1} = 0.963(1 - e^{-\Delta \ln(\frac{N}{\pi}\sin(\frac{n\pi}{N}))}) \tag{59}$$

for $N = 300$ and $\Delta = 0.067$. Using (59) in (43) gives the dominant eigenvalues or probabilities ($n \ll N = 300$)

$$p_l[N,n,1] \approx e^{-\Delta \ln(n)}(1 - e^{-\Delta \ln(n)})^l \tag{60}$$

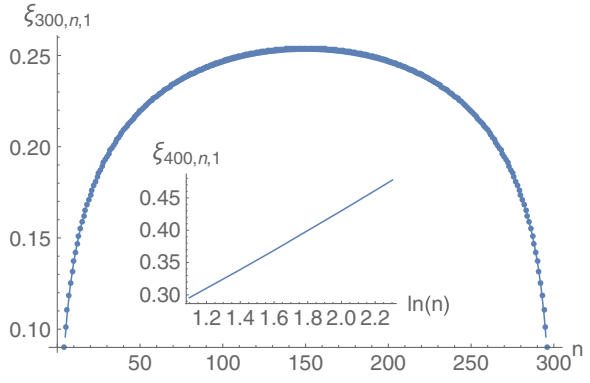

FIG. 7. Largest eigenvalue $\xi_{300,n,1}$ versus n in the full range $0 < n < 300$, with the midchain periodicity manifest: dots are the numerical results and the solid line is a best fit (59). The insert shows $\xi_{400,n,1}$ versus $\ln(n)$ in the range $3 \le n \le 10$.

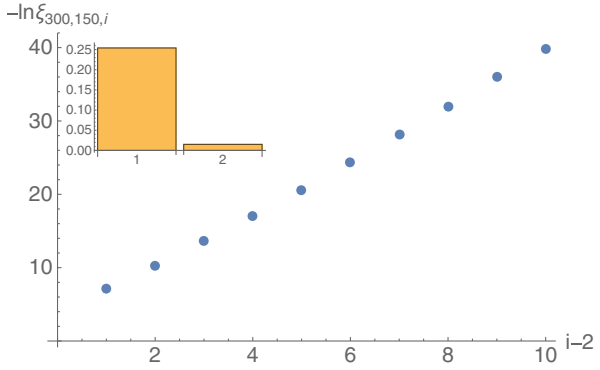

FIG. 8. Distribution of the eigenvalues $-\ln\xi_{300,150,i}$ versus $i-2$ for $3 \le i \le 12$. The insert shows the largest two eigenvalues $\xi_{300,150,i=1,2}$ on a linear scale.

with $0.963 \to 1$ for $D_\perp = 1$. For large $\ln(n)$, the numerical analysis is more intensive, but we expect $\Delta = 0.067 \to \frac{1}{6}$ as required by the entropy constraint (46).

B. Cascade equation

In general, we have $D_\perp$ independent copies of string chains, each with $l_{1,\ldots,D_\perp}$, $n_{1,\ldots,D_\perp} = n$. For fixed and common n (rapidity), and fixed $l = l_1 + \cdots + l_{D_\perp}$, the largest eigenvalue (60) is replaced by

$$\begin{aligned} p_l[D_\perp,N,n,1] &= \sum_{l=l_1+\cdots+l_{D_\perp}} \prod_{M=1}^{D_\perp} p_{l_M}[N,n,1] \\ &= \frac{(l+D_\perp-1)!}{l!D_\perp!} \\ &\quad \times e^{-D_\perp\Delta\ln(n)}(1-e^{-\Delta\ln(n)})^l \end{aligned} \tag{61}$$

which satisfies a cascade equation in rapidity

$$\frac{dp_l}{d\ln n} = -\Delta(l+1)p_l + \Delta(l+D_\perp-1)p_{l-1} \tag{62}$$

with $n = e^\chi$ following from (51). In terms of the mean $\langle l\rangle$, (61) is a negative binomial distribution

$$p_l[D_\perp,N,n,1] = P^{\rm NBD}(D_\perp,\langle l\rangle - D_\perp, l). \tag{63}$$

For $D_\perp = 1$ and modulo Δ, (63) is identical to the probability to find l-wee-dipoles inside a hadron at rapidity $\chi = \ln(n)$ following from a model of nonlinear QCD evolution at weak coupling [10].

C. Structure function at low-x

Deep inelastic ep scattering at low-x is similar to pp scattering in the Pomeron regime. The virtual photon exchange at large Q^2 in ep scattering, acts as a dipole of size $1/Q$ scattering off the proton as a quark-diquark dipole, hence the similarity. In the holographic limit, both involve the exchange of a closed surface. To map the

kinematical parameters for $\gamma^*(q)+N(p)\to\gamma^*(q)+N(p)$ we note that

$$s-m_N^2=Q^2\left(\frac{1}{x}-1\right) \tag{64}$$

with Bjorken-x defined as $x=Q^2/2p\cdot q$ and $Q^2=-q^2\geq 0$. In the Pomeron regime with $s\gg Q^2\gg -t$, we have $s\approx Q^2/x$. From the identification (51) it follows that for fixed Q^2

$$\chi=\ln s=\ln n=\ln\frac{1}{x}. \tag{65}$$

The larger the boost, the larger the rapidity, the smaller the range of Bjorken-x probed by the string transverse fluctuations. Hence, $x=\frac{1}{n}$ is identified as the fraction of longitudinal momentum carried by each of the transverse n-string bits.

It follows that the string fluctuations as wee-quanta carry longitudinal momentum, where the mean captured by the $F_2(x)$ structure function at low-x is ($n\gg N$)

$$F_2(x)\sim\sum_{l=0}^{\infty}lp_l[D_\perp,N,n,1]=D_\perp n^\Delta=\frac{D_\perp}{x^\Delta}. \tag{66}$$

The exponent Δ is fixed by the zero point motion or quantum entanglement of the string through the Pomeron intercept

$$\Delta=\frac{1}{6}\to\frac{2}{D_\perp}(\alpha_{\mathbb{P}}(0)-1) \tag{67}$$

Recall from (56) and the ensuing estimate, that the entanglement entropy saturates for $\chi_S=10.6$. Using (65), this translates to a saturation at low-x when $x_S\approx 210^{-5}$.

VI. CONCLUSIONS

In walled AdS, parton-parton scattering at large $\sqrt{s}$ is dominated by the exchange of a hyperbolic surface that Reggeizes through a world sheet instanton. The zero point motion of the string is characterized by a quantum or thermodynamical entropy $\mathcal{S}_T$ that is tied to the rise of the scattering amplitude and multiplicities in hadron-hadron scattering at large rapidities.

The surface is spatially entangled with an entanglement or von-Neumann entropy $\mathcal{S}_E$ that coincides with the quantum or thermodynamical entropy $\mathcal{S}_T$, i.e., $\mathcal{S}_T=\mathcal{S}_E$. This entanglement entropy coincides with the one in critical 2-dimensional conformal field theories and spin chains with a central charge $D_\perp$.

At asymptotic rapidities, the ratio of the entanglement entropy to the transverse area of the string is similar to that of a black hole. The string appears maximally entangled with a saturation momentum fixed by the string length. This suggests that the rate of growth of the entanglement entropy when cast in terms of Gribov diffusion time, is at the chaos bound. These observations maybe at the origin of the fast scrambling of information and collectivization in pp collisions as recently reported by the CMS collaboration [7], and argued in [33].

The largest eigenvalues of the entangled density matrix obey a cascade equation in rapidity. They describe the probability distributions of wee-quanta at low-x and strong coupling, much like the Balitsky-Fadin-Kuraev-Lipatov wee-dipoles at weak coupling. They are measurable through the multiplicities in hadron-hadron scattering or structure functions in deep-inelastic scattering at present or future colliders.

ACKNOWLEDGMENTS

This work was supported by the U.S. Department of Energy under Contract No. DE-FG-88ER40388.

[1] C. Holzhey, F. Larsen, and F. Wilczek, Nucl. Phys. **B424**, 443 (1994); T. M. Fiola, J. Preskill, A. Strominger, and S. P. Trivedi, Phys. Rev. D **50**, 3987 (1994); P. Calabrese and J. L. Cardy, J. Stat. Mech. (2004) P06002.
[2] G. Vidal, J. I. Latorre, E. Rico, and A. Kitaev, Phys. Rev. Lett. **90**, 227902 (2003).
[3] J. Maldacena and L. Susskind, Fortschr. Phys. **61**, 781 (2013).
[4] K. Jensen and A. Karch, Phys. Rev. Lett. **111**, 211602 (2013); K. Jensen, A. Karch, and B. Robinson, Phys. Rev. D **90**, 064019 (2014); J. Sonner, Phys. Rev. Lett. **111**, 211603 (2013).
[5] S. Ryu and T. Takayanagi, Phys. Rev. Lett. **96**, 181602 (2006).
[6] M. Srednicki, Phys. Rev. Lett. **71**, 666 (1993).
[7] V. Khachatryan *et al.* (CMS Collaboration), Phys. Lett. B **765**, 193 (2017).
[8] A. Stoffers and I. Zahed, Phys. Rev. D **88**, 025038 (2013); E. Shuryak and I. Zahed, Phys. Rev. D **89**, 094001 (2014).
[9] R. Peschanski, Phys. Rev. D **87**, 034042 (2013); A. Kovner and M. Lublinsky, Phys. Rev. D **92**, 034016 (2015); J. Berges, S. Floerchinger, and R. Venugopalan, Phys. Lett. B **778**, 442 (2018); Y. Hagiwara, Y. Hatta, B. W. Xiao, and F. Yuan, Phys. Rev. D **97**, 094029 (2018).

[10] D. E. Kharzeev and E. M. Levin, Phys. Rev. D **95**, 114008 (2017).
[11] V. N. Gribov, *Quark Confinement and Gauge Theories* (PHASIS, Moscow, 2002).
[12] A. Donnachie and P. V. Landshoff, Phys. Lett. B **296**, 227 (1992).
[13] I. I. Balitsky and L. N. Lipatov, Yad. Fiz. **28**, 1597 (1978) [Sov. J. Nucl. Phys. **28**, 822 (1978)].
[14] E. A. Kuraev, L. N. Lipatov, and V. S. Fadin, Zh. Eksp. Teor. Fiz. **72**, 377 (1977) [Sov. Phys. JETP **45**, 199 (1977)].
[15] M. Rho, S. J. Sin, and I. Zahed, Phys. Lett. B **466**, 199 (1999).
[16] R. A. Janik and R. B. Peschanski, Nucl. Phys. **B586**, 163 (2000); R. A. Janik, Phys. Lett. B **500**, 118 (2001); M. Giordano and R. Peschanski, J. High Energy Phys. 05 (2010) 037.
[17] G. Basar, D. E. Kharzeev, H.-U. Yee, and I. Zahed, Phys. Rev. D **85**, 105005 (2012).
[18] A. Stoffers and I. Zahed, Phys. Rev. D **87**, 075023 (2013); Y. Qian and I. Zahed, Phys. Rev. D **92**, 105001 (2015).
[19] R. C. Brower, J. Polchinski, M. J. Strassler, and C. I. Tan, J. High Energy Phys. 12 (2007) 005.
[20] E. Shuryak and I. Zahed, Phys. Rev. D **69**, 046005 (2004).
[21] J. M. Maldacena, Phys. Rev. Lett. **80**, 4859 (1998).
[22] O. Nachtmann, Ann. Phys. (N.Y.) **209**, 436 (1991); in *Cambridge 1995, Confinement Physics*, edited by H. L. Verlinde and E. P. Verlinde (2015), pp. 27–69.
[23] R. A. Janik and R. B. Peschanski, Nucl. Phys. **B625**, 279 (2002); G. Basar, D. E. Kharzeev, H. U. Yee, and I. Zahed, Phys. Rev. D **95**, 126005 (2017).
[24] M. Luscher, Nucl. Phys. **B180**, 317 (1981).
[25] E. Shuryak and I. Zahed, Ann. Phys. (Amsterdam) **396**, 1 (2018).
[26] A. H. Mueller, Nucl. Phys. **B437**, 107 (1995).
[27] M. Karliner, I. R. Klebanov, and L. Susskind, Int. J. Mod. Phys. A **03**, 1981 (1988).
[28] O. Bergman and C. B. Thorn, Nucl. Phys. **B502**, 309 (1997).
[29] L. Susskind and P. Griffin, arXiv:hep-ph/9410306; Y. Qian and I. Zahed, Phys. Rev. D **91**, 125032 (2015).
[30] J. D. Bekenstein, Phys. Rev. D **9**, 3292 (1974).
[31] A. N. Kolmogorov, Dokl. Akad. Nauk SSSR **119**, 861 (1958); **124**, 754 (1959); V. Latora and M. Baranger, Phys. Rev. Lett. **82**, 520 (1999).
[32] P. Hayden and J. Preskill, J. High Energy Phys. 09 (2007) 120; Y. Sekino and L. Susskind, J. High Energy Phys. 10 (2008) 065.
[33] E. Shuryak and I. Zahed, Phys. Rev. D **89**, 094001 (2014).